

---

# Scalable Simple Linear Iterative Clustering (SSLIC) Using a Generic and Parallel Approach

*Release 1.0*

Bradley C. Lowekamp<sup>1,2</sup> and David T. Chen<sup>1,2</sup> and Ziv Yaniv<sup>1,3</sup> and Terry S. Yoo<sup>1</sup>

July 24, 2018

<sup>1</sup>National Library Of Medicine <sup>2</sup>Medical Science and Computing LLC<sup>3</sup> TAJ Inc.

## Abstract

Superpixel algorithms have proven to be a useful initial step for segmentation and subsequent processing of images, reducing computational complexity by replacing the use of expensive per-pixel primitives with a higher-level abstraction, superpixels. They have been successfully applied both in the context of traditional image analysis and deep learning based approaches. In this work, we present a generalized implementation of the simple linear iterative clustering (SLIC) superpixel algorithm that has been generalized for n-dimensional scalar and multi-channel images. Additionally, the standard iterative implementation is replaced by a parallel, multi-threaded one. We describe the implementation details and analyze its scalability using a strong scaling formulation. Quantitative evaluation is performed using a 3D image, the Visible Human cryosection dataset, and a 2D image from the same dataset. Results show good scalability with runtime gains even when using a large number of threads that exceeds the physical number of available cores (hyperthreading).

Latest version available at the [Insight Journal](http://hdl.handle.net/10380/3596) [ <http://hdl.handle.net/10380/3596>]

Distributed under [Creative Commons Attribution License](#)

## Contents

<b>1</b>	<b>Introduction</b>	<b>2</b>
<b>2</b>	<b>The Simple Linear Iterative Clustering (SLIC) Algorithm</b>	<b>3</b>
2.1	Distances in the joint range-domain (intensity-geometry) space . . . . .	3
2.2	Algorithm Details . . . . .	4
<b>3</b>	<b>The Scalable Simple Linear Iterative Clustering (SSLIC) Algorithm</b>	<b>4</b>
3.1	Algorithm Details . . . . .	4
3.2	SSLIC Parameters . . . . .	5
3.3	Implementation Details . . . . .	6

---

<b>4</b>	<b>SSLIC Evaluation</b>	<b>6</b>
4.1	Method . . . . .	7
4.2	Results . . . . .	10
	Qualitative . . . . .	10
	Quantitative . . . . .	10
<b>5</b>	<b>Updating with Modern Threads</b>	<b>12</b>
<b>6</b>	<b>Discussion and Conclusion</b>	<b>13</b>
<b>A</b>	<b>Detailed Quantitative Results</b>	<b>17</b>

---

## 1 Introduction

Pixels, or voxels in three dimensions, are the basic primitive of an image, usually defining a rectilinear grid. Superpixels reduce the number of primitives representing an image by grouping pixels based on low level features, properties such as color, texture and physical proximity. Originally introduced in [13] as a method for reducing the complexity of higher-level image analysis tasks, they have been successfully used in many computer vision tasks such as object detection, depth estimation, and segmentation. A large number of algorithms for creating superpixels have been proposed in the literature, with a recent comparative evaluation of 28 algorithms described in [16]. One of the more popular and successful superpixel algorithms is the Simple Linear Iterative Clustering (SLIC) algorithm [1, 11].

The SLIC algorithm has been used both in the context of classical image analysis algorithms and in the context of deep learning. Examples of using SLIC in the context of graph based algorithms include segmentation of mitochondria in electron microscopy volumes [11], classification of hyperspectral images [9], segmentation of the prostate in MR [17], and segmentation of the liver in CT [19]. Examples of using the SLIC algorithm in combination with deep learning include segmentation of the pancreas in CT [6], general salient object detection in color pictures [8], hyperspectral image classification [14], detection of cell nuclei in digital histology slides [15], and classification of epithelial and stromal regions in histopathology images [20].

The National Library of Medicine’s Insight Segmentation and Registration Toolkit (ITK) includes a couple of segmentation algorithms that could be classified as superpixel methods; they are the toboggan image filter, the classic watershed image filter and the morphological watershed image filter [4]. These filters are all related to the original watershed segmentation algorithm, operate on the gradient magnitude and perform region growing with seeds from the local gradient magnitude minima. These methods are greedy algorithms and single threaded, therefore they are neither scalable for large data nor is the whole vector space taken into consideration for the superpixel grouping when the image is non-scalar.

Our contribution of a scalable version of the SLIC algorithm is motivated by work with several types of large images with a variety of characteristics. These types include focused ion-beam scanning electron microscopy (FIB-SEM) which forms 3D volumes with a single channel (gray scale). Typical image sizes are more than 4 Gb with continued demanded for increased resolution and larger volumes. Another large image type of interest is whole slide histology imaging. Histology images are generally 2D three channel (RGB) images with a size of several ( $\leq 10$ ) Gb. Finally, we are also interested in working with 3D multi-

channel confocal microscopy images whose size is also on the order of several ( $\leq 10$ ) Gb.

In the rest of this paper we describe the original SLIC algorithm, our parallel and multi-dimensional version of the algorithm, Scalable SLIC (SSLIC), and an evaluation of our algorithm's scalability using both a large 53Gb 3D color image and a comparatively small 24Mb 2D color image.

## 2 The Simple Linear Iterative Clustering (SLIC) Algorithm

Our superpixel implementation is based on the SLIC algorithm proposed by Achanta et al. [1]. The goals outlined for the SLIC algorithm include the following desirable properties with respect to the resulting superpixels and the computation process: 1) The natural boundaries of the image should be preserved by the boundaries of the superpixels. 2) Computations of the superpixels should be quick, have low memory requirements and involve only a few parameters. 3) The generated superpixels should improve the accuracy and speed of subsequent segmentation steps.

The SLIC algorithm can be viewed as a specialized and optimized variation of k-means clustering where each pixel is mapped to a point whose coordinates correspond to a concatenation of the pixel coordinates and the channel values for that pixel. The original algorithm dealt with 2D color images using the CIE-Lab color space. Thus each pixel was mapped to a five vector  $[L, a, b, x, y]$  with clustering performed in this 5D space. A user specified property of the SLIC superpixels is the expected size of the super pixel, denoted by  $S$ . This restricted size enables the reduction of the global search space of classic k-means to a local neighborhood in the image domain of size  $2S \times 2S$ .

### 2.1 Distances in the joint range-domain (intensity-geometry) space

Defining an image as  $I : \Omega \rightarrow \mathbf{r}$ , a joint range-domain (intensity-geometry) cluster center is represented as  $C' = [\Omega \mathbf{r}]^T$ . For the case of a 2D image with a CIE-Lab color representation the cluster center is  $C_k = [L, a, b, x, y]^T$ . The distance between any pixel and a cluster center is defined as  $D = \sqrt{d_c^2 + \left(\frac{d_s}{S}\right)^2 m^2}$ , where  $d_c$  and  $d_s$  are the Euclidean distance for the separate range and domain, respectfully.  $S$  is a normalizing constant which is the expected size of a cluster and  $m$  is a user specified weighting parameter. When  $m$  is reduced the  $d_c$  component becomes more dominant causing color to be the main criteria for cluster affinity while when it is increased the spatial regularity of clusters is emphasized. For 2D images of CIE-Lab color, a range of  $m \in [1, 40]$  is suggested with 10 being the default.

This distance metric can easily be extended to gray-scale images or general multi-channel images by the 2-norm of  $d_c$ . Similarly,  $d_s$  can support n-dimensional images. It is worth observing that the range of intensity values effects the weight of  $d_c$  vs. the  $d_s$  components. The CIE-Lab color space has a range of  $L \in [0, 100]$ ,  $a \in [-86.185, 98.254]$  and  $b \in [-107.863, 94.482]$ , which needs to be considered when working with normalized data or data with a 16-bit integer range. Also note that the number of components of either the color or dimension will also affect the weighting of the metric.

From a practical standpoint, the outer most square root of  $D$  is not necessary, as squared values maintain their ordering based on the squared distance. Additionally, the fortuitous use of squared Euclidean distances removes additional uses of square roots. This fact results in an actual implementation of simply the sum of the squares of the difference between the cluster center and the joint range-domain representation with a constant:  $D = (L_{C_k} - L_i)^2 + (a_{C_k} - a_i)^2 + (b_{C_k} - b_i)^2 + ((x_{C_k} - x_i)^2 + (y_{C_k} - y_i)^2) \frac{m^2}{S^2}$

## 2.2 Algorithm Details

The SLIC algorithm consists of the following three stages:

**1. Initialization:** The cluster centers  $C_k$  are initialized by regularly sampling the domain  $\Omega$  at fixed intervals. Each center is then perturbed to the location and value of the lowest gradient magnitude<sup>1</sup> in its  $3 \times 3$  neighborhood. Next, a label image,  $l$ , is initialized to an undefined label and a distance image,  $d$ , is initialized to  $\infty$ .

**2. Iterate till termination criterion satisfied:**

**Iterate over  $C_k$ :**

**Update label and distance images:** For all pixels,  $\mathbf{x}$ , in a  $[2S \times 2S]$  region around  $C_k$ , compute  $D(C_k, [I(\mathbf{x}), \mathbf{x}])$ . If this distance is less than  $d(\mathbf{x})$  update  $l(\mathbf{x}) = k$  and  $d(\mathbf{x})$ .

**Update clusters:** For all labels, compute new cluster centers based on the updated pixel labels, where the new center for cluster  $k$  is the mean of  $[I(\mathbf{x}), \mathbf{x}]$  where  $l(\mathbf{x})$  is equal to  $k$ .

**Terminate iterations if:** Distance between previous and current cluster centers is below a threshold or we have reached the maximal number of iterations.

**3. Spatial connectivity enforcement:** Connectivity is not enforced in the above steps so the cluster may not be fully connected for all components. This post processing step examines labeled connected components not connected to their cluster center. Such a connected component is relabeled so that it is connected to the "nearest" label, or if the component is of sufficient size, it is assigned a new label.

## 3 The Scalable Simple Linear Iterative Clustering (SSLIC) Algorithm

Two key principles guiding ITK algorithm development are that: (a) algorithms should be designed to work with n-dimensional images having an arbitrary number of channels per pixel, and (b) algorithms should take advantage of modern hardware to parallelize computations. Our proposed SSLIC algorithm follows both principles in a manner which satisfies the goals of the original algorithm while focusing on significantly improving its speed. In addition, SSLIC generalizes the original algorithm to n-dimensional images with an arbitrary number of channels per pixel. We next describe our approach to implementing the SLIC algorithm in a parallel manner.

### 3.1 Algorithm Details

The SSLIC algorithm consists of the following three stages:

**1. Initialization:** The cluster centers  $C_k$  are initialized by regularly sampling the domain  $\Omega$  at fixed intervals. Then all cluster centers are updated in parallel so that they are moved to the lowest gradient magnitude location in the  $3 \times 3$  neighborhood of their original locations. Next, a label image,  $l$ , is initialized to an undefined label and a distance image,  $d$ , is initialized to  $\infty$ .

<sup>1</sup>This gradient only applies when dealing with single channel images. When the image has multiple channels we use the Frobenius norm of the Jacobian matrix ( $\|J\|_F \equiv \sqrt{\sum_{i=1}^m \sum_{j=1}^n J_{i,j}^2}$ ).

## 2. Iterate till termination criterion satisfied:

### Create non-overlapping regions which split the image and update label and distance images in parallel:

Iterating over  $C_k$ , if the cluster's  $[2S \times 2S \dots 2S]$  nD neighborhood intersects the region assigned to the thread, for all pixels,  $\mathbf{x}$ , in this intersection, compute  $D(C_k, [I(\mathbf{x}), \mathbf{x}])$ . If this distance is less than  $d(\mathbf{x})$  update  $l(\mathbf{x}) = k$  and  $d(\mathbf{x})$ .

### Create non-overlapping regions which split the image and update $C_k$ using a map-reduce scheme:

Map - in each region iterate over the pixels and accumulate the joint intensity-geometry information per label. Reduce - merge the information from all regions based on the label ids and update the cluster centers where the new center for cluster  $k$  is the mean of the joint intensity-geometry information obtained for label  $k$  in the previous step.

**Terminate iterations if:** We have reached the maximal number of iterations (distance between previous and current cluster centers is computed and available).

## 3. Spatial connectivity enforcement:

**Initialize** a marker image  $m$  to a value indicating that the label at that location is not the final label.

**In parallel** for each cluster center, if the label at the location defined by  $C_k$  is equal to  $k$  (our cluster is not torus shaped), or we found the label  $k$  in the  $[S \times S \dots S]$  nD neighborhood centered on  $C_k$ , obtain the connected component with label  $k$  using this initial seed point. If this connected component's size is greater than  $\frac{S^n}{4}$ , update the maker image in all these locations to indicate the label is final.

**Iterate over  $m$** , if  $m(\mathbf{x})$  is not final, obtain the connected component with label  $l(\mathbf{x})$  using  $\mathbf{x}$  as the seed point. If the size of this connected component is larger than  $\frac{S^n}{4}$ , change the label image for all these locations to a new label,  $k + 1$ , otherwise change it to the last encountered label and update the marker image to indicate that the label is final.

## 3.2 SSLIC Parameters

The SSLIC filter exposes two user adjustable parameters of interest: the desired super grid size and the spatial weight factor which balances between superpixel spatial regularity and color affinity.

The desired grid size in the original SLIC algorithm was a single number which is appropriate for isotropic pixels. As our goal is to accommodate images from a variety of sources, many of which are highly unisotropic, we allow the the size of the superpixel to be specified as the number of pixels in each dimension i.e.  $[S_x, S_y, S_z]$ . Therefore the superpixels themselves can be anisotropic to accommodate non-uniform pixel spacing, as is common in medical images.

The weight factor is utilized to balance between the spatial and image intensity portions of the distance metric. The default value is 10, which provides good results for 2D images in the CIE-Lab color space. Increasing the value increases the weight of the spatial component which produces more regularly shape and sized superpixels. Image dimensionality, and similarly the magnitude of the range of the pixels values will effect the relative weight between the two components of the distance metric and may require experimentation to identify the relevant weighting for a specific setting ( $nD$  image with  $c$  channels per pixel).

Additionally, the user can specify the algorithm's termination criteria via the maximal number of iterations, while the residuals or the change in cluster centers between two consecutive iterations can be monitored. The maximum number of iterations defaults to 5 for images with dimension 3 or greater, whereas the original SLIC implementation specifies 10 iterations for 2D images.

### 3.3 Implementation Details

Achieving the goals of memory and computational efficiency, while still supporting grayscale, fixed vector and dynamic vector images requires some planning and prudent choices for data-structures and memory layout. The resulting output  $l$  is clearly a label image, and the intermediate per pixel distance values,  $d$ , are also represented by an image. Efficiently supporting variable length vectors in ITK can be challenging due to the potential memory allocation per pixel to support the run-time length. To avoid this, we store the set of cluster centers, whose lengths are the number of dimensions plus the number of components for the pixel value, in a single 1-dimensional array. The values of a cluster  $C_k$  are simple accessed via a 'vnl\_ref\_vector', which references the data in the array.

The user provided superpixel grid size specifies the expected size in pixel units, not physical units as is common in ITK. The use of pixel units enables the grid size parameter to be independent of the image spacing, removes potential degenerate cases, allows reasonable default values, and follows that the superpixels are an abstraction from the pixels. Therefore the "distance" metric computed must be computed in index space and not physical space. We have also extended the grid size to potentially be isotropic. So the spatial weights are applied thusly:  $D = \sqrt{d_c^2 + \sum_i \left(\frac{d_i}{s_i}\right)^2} m^2$ .

## 4 SSLIC Evaluation

As the focus of our algorithm was on improving the runtime of the original SLIC algorithm without changing the original algorithmic approach we limit our evaluation to computational performance and scalability.

In general, the time it takes to perform a task is comprised of the time it takes to complete its sequential portion and the time it takes to perform its parallel portion:

$$T = T_s + T_p$$

In our evaluation we use the concept of strong scalability. That is, the problem size is kept fixed while we increase the number of parallel process (in our case these are lightweight threads).

The relative speedup<sup>2</sup> obtained by using more than a single process is defined as:

$$S(p) = \frac{T(1)}{T(p)}, \text{ where } T(1) \text{ is the runtime of the parallel implementation using a single process.}$$

The optimal relative speedup value is  $S^*(p) = p$ .

The relative efficiency is defined as speedup divided by the number of processors:

$$E(p) = \frac{S(p)}{p}$$

The optimal relative efficiency is thus  $E^*(p) = 1$ .

When evaluating using strong scalability we have an upper bound on the possible relative speedup and efficiency which are given by Amdahl's law [3]. Given that a fraction,  $\alpha \in [0, 1]$ , of the task is serial we

<sup>2</sup>"Relative speedup" uses the single process implementation of the parallelized algorithm and not the best sequential algorithm which would correspond to "speedup".

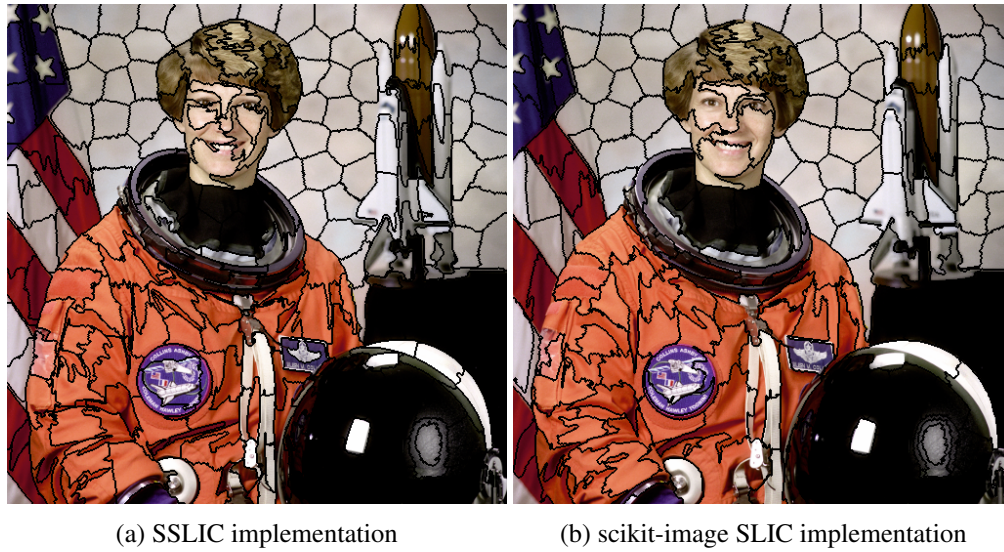


Figure 1: Comparison of our SSLIC implementation and the scikit-image [18] SLIC implementation on a  $512 \times 512$  color image converted to CIE-Lab color space. Each implementation was run for 10 iterations and the size of the superpixels was specified as  $[32 \times 32]$  for our implementation, and a requested number of superpixels of 256 for scikit-image. The runtimes for our implementation were 292ms, 86ms, and 52ms with 1, 4 and 8 threads respectively, while scikit-image’s single threaded implementation runtime was 166ms.

have:

$$S(p) = \frac{T(1)}{\alpha T(1) + (1 - \alpha)T(p)} \leq \frac{1}{\alpha + (1 - \alpha)/p}$$

and

$$E(p) = \frac{T(1)}{p(\alpha T(1) + (1 - \alpha)T(p))} \leq \frac{1}{1 + \alpha(p - 1)}$$

#### 4.1 Method

To evaluate the performance of the SSLIC algorithm we utilize the cyrosection Visible Human Male dataset [2]. A frozen male cadaver which was serially imaged and sectioned at 1 millimeter intervals to form The color volume Visible Human of  $[2048 \times 1216 \times 1978]$  voxels. The size of the original RGB (unsigned char) volume is 16Gb, and 53 Gb after conversion to CIE-Lab (float), which is the data used in this work. A single 2D slice is evaluated in addition to the whole volume to enable performance comparison at two problem set sizes.

The computer system used for the performance analysis is a two CPU socket server running Red Hat Enterprise Linux Server release 7.5. The CPUs are Intel Zeon CPU E5-2699 v4 @2.20GHz each having 22 physical cores and Hyper-Threading enabled, resulting in 44 physical cores or 88 virtual cores. The system has 512 Gigabytes of memory which is sufficient for processing the dataset without swapping to disk.

To analyze the scalability of the SSLIC algorithm, the time of execution is measured for a fixed image while varying the number of threads allocated to the task. This was implemented in a python script via SimpleITK bindings [10]. The reported timing is of the SimpleITK `Execute` method which includes the

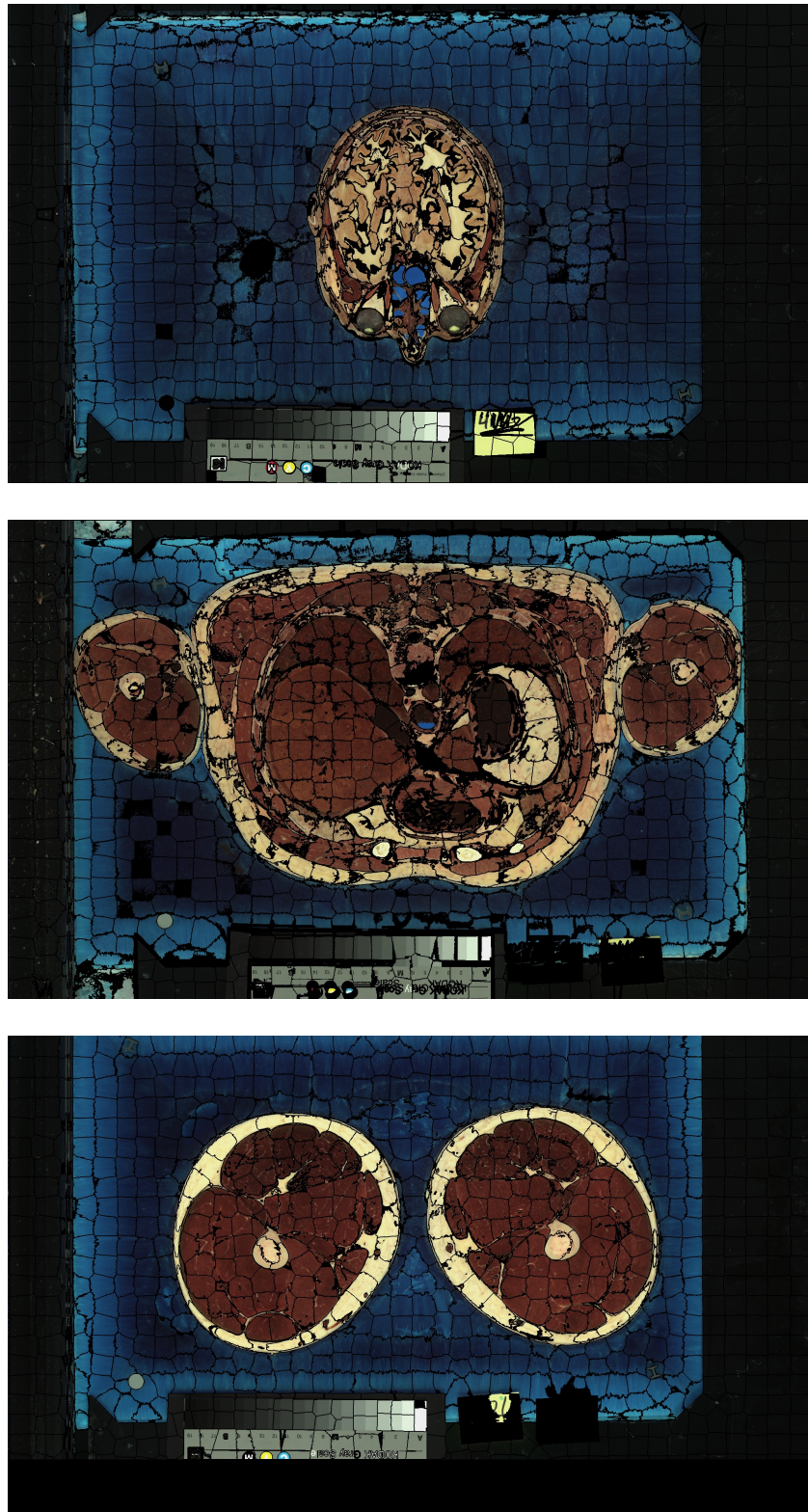


Figure 2: Selected slices of the Visible Human Male (110,487,116) with rendered superpixel borders. The SSLIC parameters were super grid  $[30 \times 30 \times 10]$ , spatial weight 10, and 5 iterations. The color slices were converted to CIE-Lab color space. The algorithm and superpixels are in 3D, so black regions may be caused by co-planar slice and superpixel boundaries.

Latest version available at the [Insight Journal](http://hdl.handle.net/10380/3596) [ <http://hdl.handle.net/10380/3596> ]

Distributed under [Creative Commons Attribution License](https://creativecommons.org/licenses/by/4.0/)



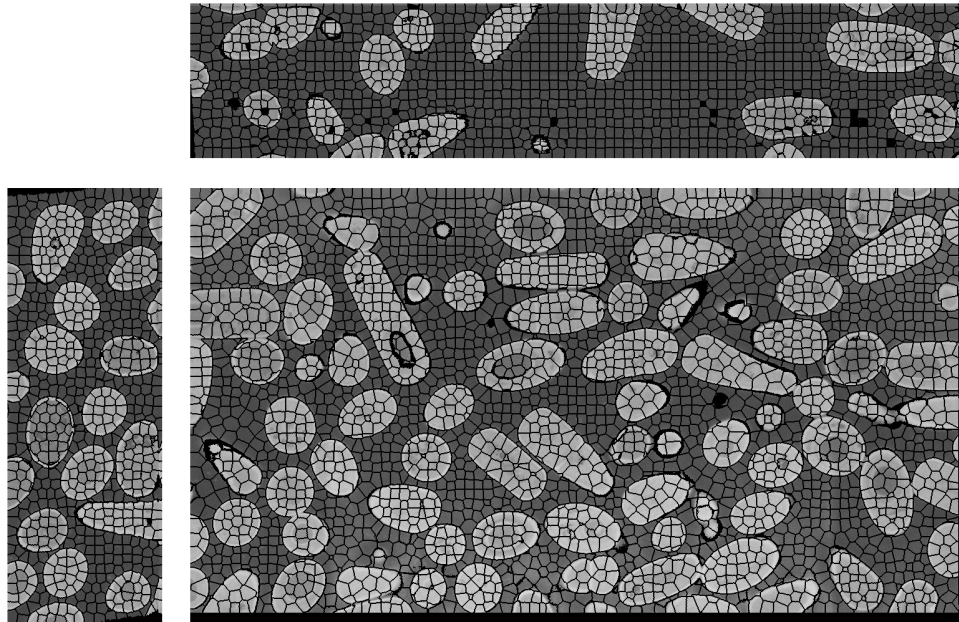


Figure 3: Planar cross sections of *Bacillus subtilis* acquired with focused ion-beam scanning electron microscopy. The SLIC parameters were super grid  $[15 \times 15 \times 15]$  spatial weight 5, and 10 iterations. From the  $[1243 \times 2094 \times 247]$  volume a selected X-Y planar slice is on the lower right, a Y-Z slice is on the left, and an X-Z slice is at the top.

construction and setting of ITK parameters therefore this approach adds some negligible constant overhead when compared to directly executing the ITK filter. The execution is timed with and without the connectivity enforcement step. As this post-processing step involves a single threaded pass through the entire image, the separate timings enables the scalability assessment of the two algorithmic stages independently.

The code was built against the latest stable ITK release 4.13.0 with C++11 enabled for improved compatibility with the forthcoming ITK 5.0 release. The system compiler, "gcc (GCC) 4.8.5 20150623 (Red Hat 4.8.5-28)" was used with the default ITK flags for "release" mode.

The method was first executed on the extracted 100th slice of the Visible Human with dimensions of  $[2048 \times 1216]$  pixels. The SSLIC algorithm ran for 5 iterations with an isotropic supergrid size of 50, and the default spatial weight of 10. This test case was executed 5 times, and the minimum time is reported. With the brief execution time of less than a second, the number of threads allocated to the SSLIC was incremented by 1.

Next the algorithm was evaluated on the whole 53 Gigabyte 3D Visible Human dataset. The same parameters were specified: 5 iterations, 50 supergrid size, and spatial weight 10. The algorithm was only run once for a selection of number of threads.

Visualization of the resulting multi-label segmentation image is done with a brief line of SimpleITK code (see below). Since the label ID or value of the result contains no significant meaning, only the boundaries of the superpixels are important, we follow the convention to render images using a black contour around the segmentation.

```
def mask_label_contour(image, seg):
    """Combine an image and segmentation by masking the segmentation contour.
```

```
For an input image (scalar or vector), and a multi-label
segmentation image, creates an output image where the contour of
each label masks the input image to black. """
```

```
return sitk.Mask(image, sitk.LabelContour(seg+1)==0)
```

## 4.2 Results

The following two sections describe our qualitative and quantitative evaluation of SSLIC. Superpixel labeled images are included for qualitative evaluation from a selection of datasets to represent some of the diverse image types the SSLIC algorithm is capable of operating upon. The quantitative sections focus on analyzing the performance and scalability characteristics of our implementation.

### Qualitative

We demonstrate the results of our method on 3 distinct and representative datasets. First is a photographic example of an astronaut in figure 1 from the scikit-image[18] project. Visually, both implementations yield similar results. In figure 2, three extracted slices from the 3D Visible Human dataset are shown with 3D superpixels overlaid onto the slices. To capture the anisotropic voxel size of  $[0.3 \times 0.3 \times 1.0]mm$ , the super grid size was specified as  $[30 \times 30 \times 10]$ , with the default spatial proximity of 10 and 5 iterations. The last dataset is a 3D focused ion-beam scanning electron microscopy (FIB-SEM) of *Bacillus subtilis* bacterium courtesy of the High Resolution Electron Microscopy at the National Cancer Institute, National Institutes of Health [12]. The SSLIC algorithm was run on a processed scalar volume of  $[1243 \times 2094 \times 247]$  pixel with spacing of approximately  $[12 \times 12 \times 12]nm$ , see figure 3

### Quantitative

The detailed SSLIC performance timing results for the 2D slice are given in table 1 and those for the 3D volume are in table 2. Included in the tables are the computed relative efficiency and relative speedup as defined above. These timing measurements are also summarized in figures 4 and 5.

The 2D speedup graph shows the upper bound for speedup being approached demonstrating Amdahl's law. That is to say for this relatively small 2D image we are bounded by the single threaded execution and overhead of the algorithm. This is in contrast to the continued speedup for the 1978 times larger 3D dataset. Performance gains continue when more resources are allocated to the problem. The efficiency best quantifies the difference between 2D and 3D at 44 physical cores, where the 2D case has 35% while the 3D case has 66% computed relative efficiency. The phenomena of improved efficiency on larger datasets is described by Gustafson's law[7].

When the number of cores exceeds the number of physical cores, or when HyperThreading is needed for virtual thread execution (although always enabled on the system during evaluation), the results are separated into a bar graph in figure 4. The HyperThreaded cores are a distinct type of resource from a physical core as the virtual cores share many of the same CPU physical resources such as cache and execution instructions with another. The addition of virtual cores is not expected to provide similar scalability as additional physical cores. Despite low efficiency or utilization of the virtual cores, our results demonstrate that utilizing

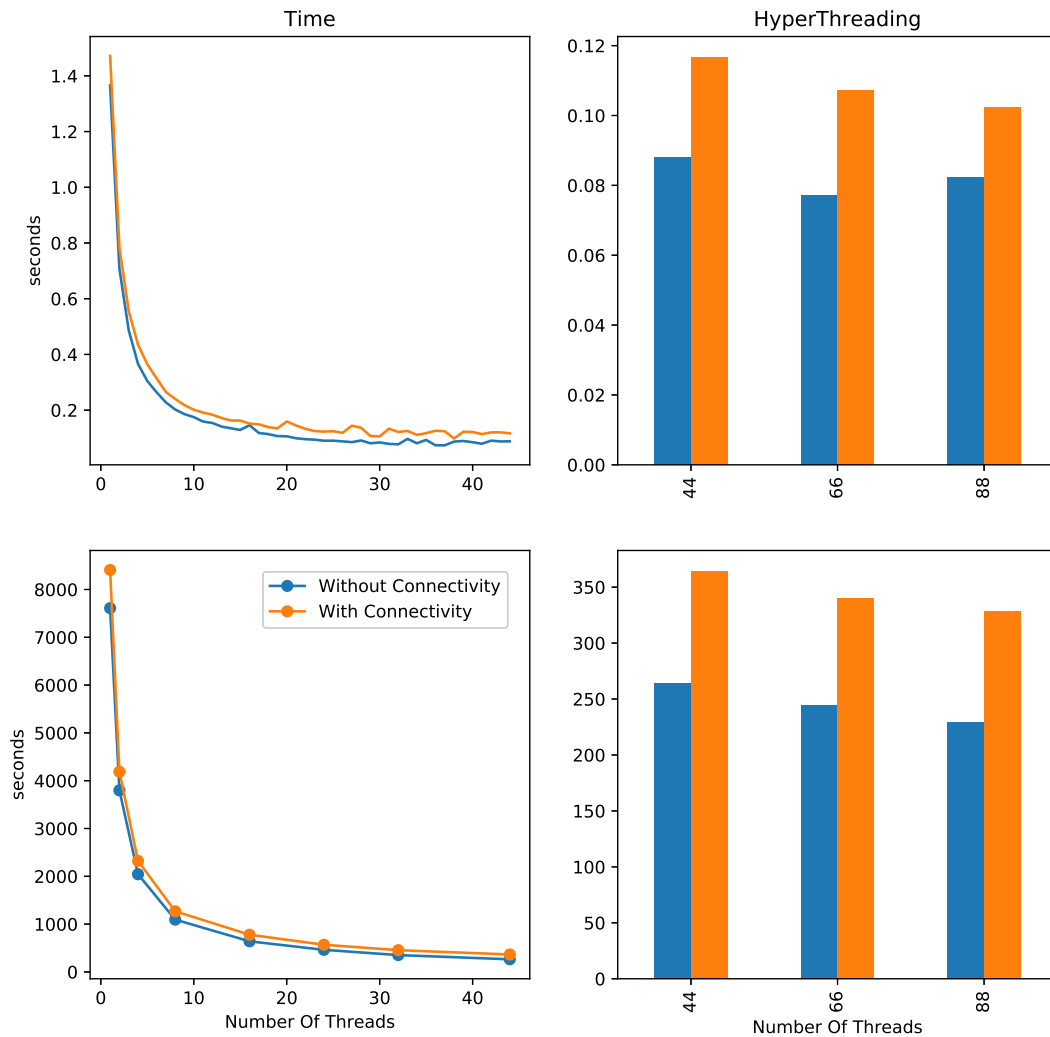


Figure 4: Execution times of the ITK SSLIC filter with a varied number of threads demonstrating SSLIC's scalability. Top row: results obtained using a single 2D slice of the Visible Human Male with  $[2048 \times 1216]$  pixels. Bottom row: results obtained using the full 3D cyrosection dataset at  $[2048 \times 1216 \times 1978]$ .

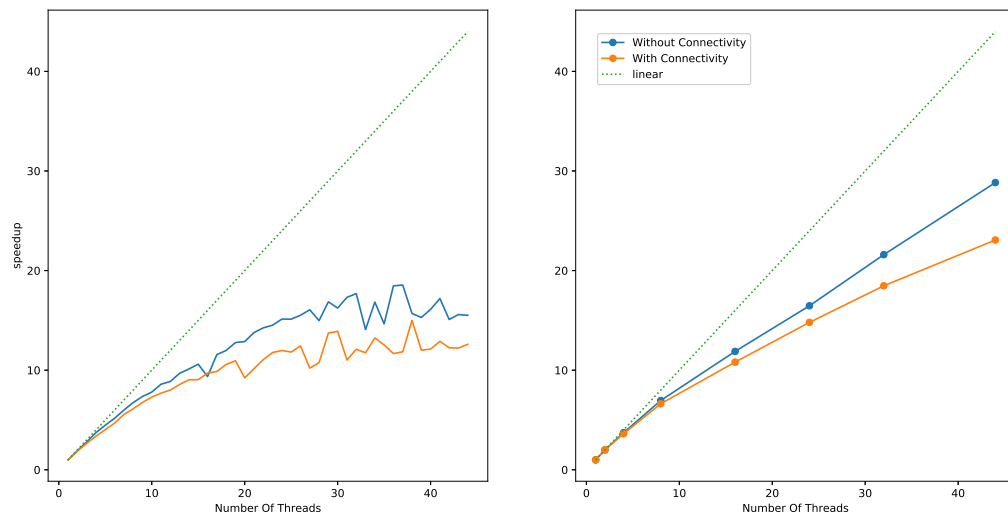


Figure 5: Speedup obtained by the ITK SSLIC filter with a varied number of threads. Comparison of the scalability on a 2D slice (left) and the 3D volume (right). The ideal linear speed up is a green dotted line.

HyperThreading yields improved performance and decreased execution time even in the extreme case with 88 threads.

## 5 Updating with Modern Threads

The forthcoming ITK version 5.0 release includes a number of performance enhancements to modernize the classic ITK threading model. The additions include multiple threading back ends such as a thread-pool and an Intel Threading Building Blocks (TBB) multi-threader interface. The latter supports dynamic load balancing and advanced task scheduling. Our initial development of SSLIC targeted the ITK version 4 interface. These emerging threading features were considered during the initial SSLIC implementation which enabled updates to support the new threading models.

The SSLIC implementation is updated to use the ITK version 5 threading model while leaving the description of the parallelism identical. The implementation changes from using thread barriers in the `ThreadedGenerateData` method to a single threaded `GenerateData` method, which invokes the new `ParallelizeArray` and `ParallelizeImageRegion` methods for each parallel step as appropriate. Additionally, a mutex lock is introduced to control access for the accumulation of the updated clusters. With this updated implementation, thread identifiers and persistent per thread allocated storage are removed from the multi-threaded step methods.

To evaluate the performance of this update the same 88 core system with the same GCC 4.8.5 compiler applied to the same extracted 100th slice of the Visible Human with dimensions of  $[2048 \times 1216]$  pixels is analyzed. The ITK code at hash '5470170e' is used for the original version of the SSLIC filter, and the update to the modern ITKv5 threading model is applied. The SSLIC algorithm timed performance is sampled 20 times, an increase to account for sensitivity in the ratio used in the speedup formula. The reported time is the minimum of 20 executions for the algorithm. We run both the original version and

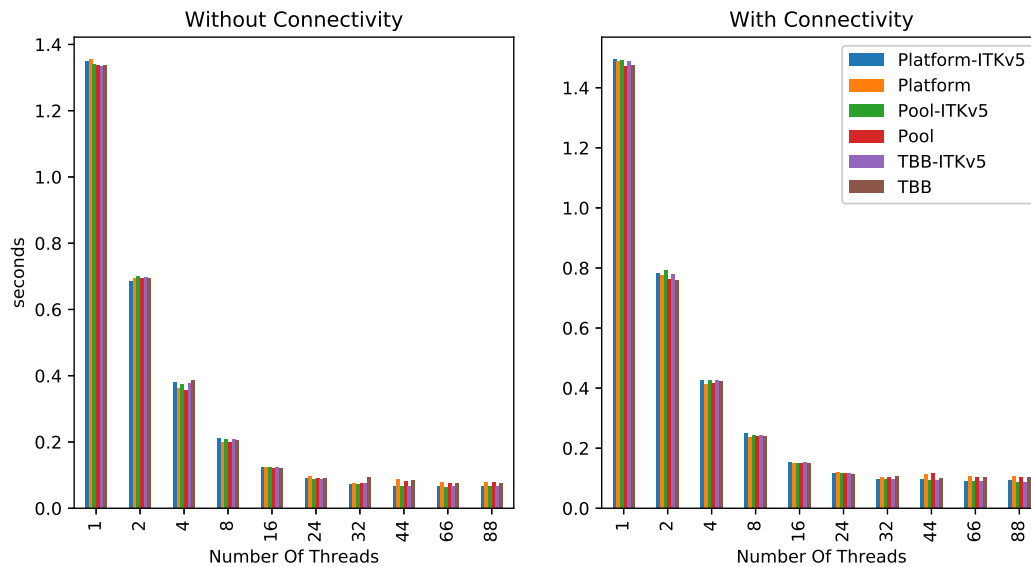


Figure 6: Execution times of the SSLIC filter with a varied number of threads, the original ITKv4 implementation, the ITKv5 implementation, and varied with the different ITK multi-threaders using a single 2D slice of the Visible Human Male with  $[2048 \times 1216]$  left: without the connectivity step right: with the connectivity step that has a significant single threaded component.

the new ITKv5 implementation for the three supported multi-threaders: Intel TBB, thread pool, and native platform (Table 3, 4). To quantify the performance difference of the new implementation we look at the speedup of the ITKv5 update by the ratio of times: *original time/new time*. Also the speed up of ITKv5 implementation compared to the classic platform multi-threader is evaluated (Table 5, 6).

The timing results are summarized in Figure 6. Overall the performance is quite similar with regard to scalability and efficiency. However, with four or eight threads the timing is marginally faster for the original implementation, while with more than 44 threads the ITKv5 implementation has a slight advantage. This is reflected in Figure 7; we conjecture that the use of a barrier in the original implementation exhibited poor scalability, while the increase in the number of dynamic memory allocations is likely responsible for the decrease in performance with the ITKv5 implementation. Further testing and profiling is required to verify these conjectures.

## 6 Discussion and Conclusion

In this work we presented SSLIC, an ITK based extension of the SLIC algorithm that accommodates n-dimensional scalar and multi-channel images and parallelizes the original sequential implementation. Using a multi-core system we have shown that our implementation has strong scalability characteristics and is able to efficiently utilize additional computational resources. When compared to the SLIC implementation found in the scikit-image toolkit [18] we observed that on a 2D image (Figure 1) our single threaded SSLIC was slower than the scikit-image SLIC, 315ms vs. 166ms, but when using additional threads it was faster, at 86ms for 4 threads and 52ms for 8 threads.

The closest work to ours is that presented in [5] which describes jSLIC, a SLIC plugin for the ImageJ

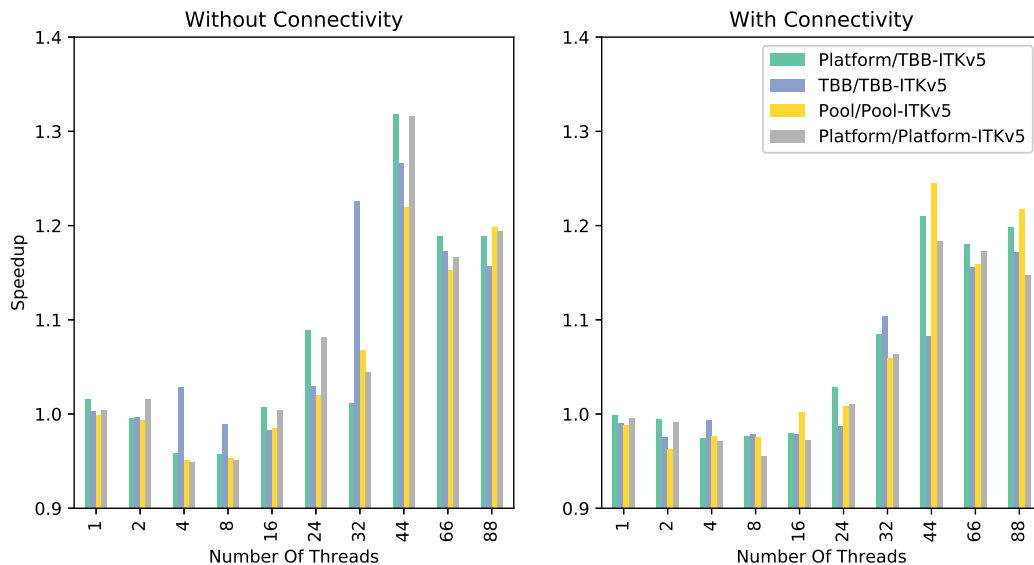


Figure 7: Speedup obtained by the ITK SSLIC algorithm with the ITKv5 implementation compared to the original with a varied number of threads. Left: without the connectivity step; right: with the connectivity step that has a significant single threaded component.

program. That work described a parallel implementation of the SLIC algorithm for color images. Beyond the parallelization, the jSLIC implementation describes a lookup table approach to conversion from RGB to CIE-Lab color space. As ITK does not explicitly support the notion of color spaces, both RGB and CIE-Lab images are three channel images. We assume the image is in CIE-Lab space when using the default weighting parameter value, otherwise the user needs to set it appropriately or convert the image to CIE-Lab representation. An additional significant difference is that the jSLIC algorithm only supports 2D images while SSLIC supports n-dimensional images. The evaluation of the jSLIC method was carried out on a 4 core machine with 8Gb RAM, with improved performance when using up to 4 threads. In our case we observed improved performance even when exceeding the number of physical cores on our system. Based on the graphs in the jSLIC paper it appears that the relative efficiency for 2 and 4 threads is approximately 0.71 and 0.45 for an image of size  $[8000 \times 8000]$  while the SSLIC implementation shows better scalability with relative efficiency for 2 and 4 threads of 0.94 and 0.84 on an image of size  $[2048 \times 1216]$ .

We presented a scalable implementation of the SLIC algorithm, SSLIC, a useful addition to ITK. We demonstrated its performance both qualitatively and quantitatively on diverse datasets of 2D and 3D, scalar and multi-component, as well as 2-dimensional and 3-dimensional images.

The SSLIC implementation is available in ITK version 5 in the SuperPixel module ([https://itk.org/Doxygen/html/group\\_\\_ITKSuperPixel.html](https://itk.org/Doxygen/html/group__ITKSuperPixel.html)), in ITK version 4.13.1 it is available in the SimpleITK-Filters remote module (<https://github.com/SimpleITK/ITKSimpleITKFilters>), and it was originally implemented in a standalone remote module (<https://github.com/blowekamp/itkSuperPixel>).

## Acknowledgments

This work was supported by the Intramural Research Program of the U.S. National Institutes of Health, National Library of Medicine.

## References

- [1] Radhakrishna Achanta, Appu Shaji, Kevin Smith, Aurélien Lucchi, Pascal Fua, and Sabine Süsstrunk. SLIC superpixels compared to state-of-the-art superpixel methods. *IEEE Trans. Pattern Anal. Mach. Intell.*, 34(11):2274–2282, 2012. [1](#), [2](#)
- [2] Michael J. Ackerman. The visible human project™: A resource for anatomical visualization. In *MEDINFO '98 - 9th World Congress on Medical Informatics, Seoul, South Korea, August 14-21, 1998.*, pages 1030–1032, 1998. [4.1](#)
- [3] Gene M. Amdahl. Validity of the single processor approach to achieving large scale computing capabilities. In *Proceedings of the April 18-20, 1967, Spring Joint Computer Conference*, pages 483–485, New York, NY, USA, 1967. ACM. [4](#)
- [4] R. Beare and G. Lehmann. The watershed transform in ITK - discussion and new developments. *Insight Journal*, 06 2006. [1](#)
- [5] Jiri Borovec and Jan Kybic. jSLIC: superpixels in ImageJ. In *19'th Computer Vision Winter Workshop*, pages 14–18. 2014. [6](#)
- [6] Amal Farag, Le Lu, Holger R. Roth, Jiamin Liu, Evrim Turkbey, and Ronald M. Summers. A bottom-up approach for pancreas segmentation using cascaded superpixels and (deep) image patch labeling. *IEEE Trans. Image Processing*, 26(1):386–399, 2017. [1](#)
- [7] John L. Gustafson. Reevaluating amdahl's law. *Commun. ACM*, 31(5):532–533, May 1988. [4.2](#)
- [8] Shengfeng He, Rynson W. H. Lau, Wenxi Liu, Zhe Huang, and Qingxiong Yang. Supercnn: A superpixelwise convolutional neural network for salient object detection. *International Journal of Computer Vision*, 115(3):330–344, 2015. [1](#)
- [9] Sen Jia, Bin Deng, Jiasong Zhu, Xiuping Jia, and Qingquan Li. Superpixel-based multitask learning framework for hyperspectral image classification. *IEEE Trans. Geoscience and Remote Sensing*, 55(5):2575–2588, 2017. [1](#)
- [10] Bradley C. Lowekamp, David T. Chen, Luis Ibáñez, and Daniel Blezek. The design of SimpleITK. *Front Neuroinform.*, 7:1–14, 2013. [4.1](#)
- [11] Aurélien Lucchi, Kevin Smith, Radhakrishna Achanta, Graham Knott, and Pascal Fua. Supervoxel-based segmentation of mitochondria in EM image stacks with learned shape features. *IEEE Trans. Med. Imaging*, 31(2):474–486, 2012. [1](#)
- [12] Kedar Narayan and Sriram Subramaniam. Focused ion beams in biology. *Nature Reviews Clinical Oncology*, 12(11):1021–1031, 11 2015. [4.2](#)
- [13] Xiaofeng Ren and Jitendra Malik. Learning a classification model for segmentation. In *9th IEEE International Conference on Computer Vision (ICCV)*, pages 10–17, 2003. [1](#)

- [14] Cheng Shi and Chi-Man Pun. Superpixel-based 3D deep neural networks for hyperspectral image classification. *Pattern Recognition*, 74:600–616, 2018. [1](#)
- [15] Sudhir Sornapudi, Ronald Stanley, William Stoecker, Haidar Almubarak, Rodney Long, Sameer Antani, George Thoma, Rosemary Zuna, and Shelliane Frazier. Deep Learning Nuclei Detection in Digitized Histology Images by Superpixels. *Journal of Pathology Informatics*, 9(1), 2018. [1](#)
- [16] David Stutz, Alexander Hermans, and Bastian Leibe. Superpixels: An evaluation of the state-of-the-art. *Computer Vision and Image Understanding*, 166:1–27, 2018. [1](#)
- [17] Zhiqiang Tian, Lizhi Liu, Zhenfeng Zhang, and Baowei Fei. Superpixel-based segmentation for 3D prostate MR images. *IEEE Trans. Med. Imaging*, 35(3):791–801, 2016. [1](#)
- [18] Stéfan van der Walt, Johannes L. Schönberger, Juan Nunez-Iglesias, François Boulogne, Joshua D. Warner, Neil Yager, Emmanuelle Gouillart, Tony Yu, and the scikit-image contributors. scikit-image: image processing in Python. *PeerJ*, 2:e453, 6 2014. [1](#), [4.2](#), [6](#)
- [19] Weiwei Wu, Zhuhuang Zhou, Shuicai Wu, and Yan-hua Zhang. Automatic liver segmentation on volumetric CT images using supervoxel-based graph cuts. *Comp. Math. Methods in Medicine*, 2016:9093721:1–9093721:14, 2016. [1](#)
- [20] Jun Xu, Xiaofei Luo, Guanhao Wang, Hannah Gilmore, and Anant Madabhushi. A deep convolutional neural network for segmenting and classifying epithelial and stromal regions in histopathological images. *Neurocomputing*, 191:214–223, 2016. [1](#)



## A Detailed Quantitative Results

Table 1: SSLIC performance as a function of number of threads using 2D color (CIE-Lab) image.

Number of Threads	Without Connectivity			With Connectivity		
	Time (sec)	Efficiency	Speedup	Time (sec)	Efficiency	Speedup
1	1.36556	1.00000	1.00000	1.47129	1.00000	1.00000
2	0.70759	0.96493	1.92987	0.78412	0.93818	1.87636
3	0.48683	0.93501	2.80503	0.55535	0.88310	2.64931
4	0.36599	0.93278	3.73112	0.43546	0.84467	3.37870
5	0.30471	0.89630	4.48152	0.36437	0.80759	4.03793
6	0.26402	0.86204	5.17222	0.31430	0.78019	4.68116
7	0.22798	0.85569	5.98984	0.26488	0.79351	5.55455
8	0.20228	0.84387	6.75099	0.24005	0.76613	6.12904
9	0.18564	0.81735	7.35614	0.21754	0.75148	6.76330
10	0.17500	0.78030	7.80304	0.20157	0.72992	7.29917
11	0.15891	0.78122	8.59343	0.19124	0.69940	7.69337
12	0.15398	0.73902	8.86822	0.18363	0.66769	8.01233
13	0.14088	0.74561	9.69296	0.17173	0.65902	8.56729
14	0.13489	0.72314	10.12391	0.16276	0.64569	9.03963
15	0.12877	0.70699	10.60492	0.16257	0.60334	9.05011
16	0.14586	0.58514	9.36222	0.15151	0.60694	9.71101
17	0.11807	0.68032	11.56552	0.14903	0.58073	9.87243
18	0.11399	0.66553	11.97957	0.13919	0.58723	10.57005
19	0.10692	0.67222	12.77220	0.13443	0.57605	10.94503
20	0.10609	0.64359	12.87189	0.15939	0.46152	9.23045
21	0.09910	0.65618	13.77981	0.14493	0.48340	10.15144
22	0.09583	0.64770	14.24930	0.13295	0.50301	11.06623
23	0.09406	0.63121	14.51783	0.12498	0.51181	11.77172
24	0.09026	0.63041	15.12986	0.12287	0.49894	11.97444
25	0.09029	0.60495	15.12367	0.12446	0.47285	11.82137
26	0.08801	0.59680	15.51671	0.11829	0.47840	12.43828
27	0.08501	0.59495	16.06374	0.14416	0.37800	10.20587
28	0.09119	0.53482	14.97491	0.13670	0.38438	10.76266
29	0.08097	0.58155	16.86505	0.10722	0.47319	13.72264
30	0.08412	0.54114	16.23411	0.10582	0.46346	13.90394
31	0.07887	0.55849	17.31305	0.13351	0.35548	11.01989
32	0.07720	0.55279	17.68938	0.12155	0.37825	12.10400
33	0.09699	0.42666	14.07986	0.12527	0.35589	11.74448
34	0.08110	0.49522	16.83738	0.11108	0.38956	13.24519
35	0.09318	0.41871	14.65498	0.11740	0.35806	12.53204
36	0.07395	0.51295	18.46609	0.12608	0.32414	11.66921
37	0.07362	0.50131	18.54832	0.12421	0.32014	11.84518
38	0.08703	0.41293	15.69130	0.09809	0.39473	14.99982
39	0.08930	0.39210	15.29205	0.12244	0.30812	12.01669
40	0.08479	0.40264	16.10579	0.12145	0.30286	12.11455
41	0.07942	0.41938	17.19465	0.11399	0.31481	12.90719
42	0.09049	0.35931	15.09095	0.12015	0.29157	12.24593
43	0.08762	0.36243	15.58452	0.12035	0.28431	12.22516
44	0.08804	0.35250	15.51003	0.11677	0.28636	12.59977
45	0.08901	0.34094	15.34222	0.11943	0.27377	12.31966
46	0.08561	0.34677	15.95140	0.11862	0.26965	12.40368

Number of Threads	Without Connectivity			With Connectivity		
	Time (sec)	Efficiency	Speedup	Time (sec)	Efficiency	Speedup
47	0.08151	0.35646	16.75376	0.11646	0.26879	12.63310
48	0.08403	0.33854	16.24996	0.11613	0.26394	12.66920
49	0.08603	0.32394	15.87311	0.11563	0.25967	12.72377
50	0.08352	0.32699	16.34973	0.11452	0.25694	12.84689
51	0.08592	0.31163	15.89289	0.11054	0.26097	13.30953
52	0.08289	0.31683	16.47540	0.10923	0.25902	13.46925
53	0.08224	0.31328	16.60402	0.10797	0.25711	13.62694
54	0.07924	0.31915	17.23413	0.11160	0.24415	13.18404
55	0.08319	0.29847	16.41576	0.10735	0.24919	13.70530
56	0.08023	0.30395	17.02122	0.10753	0.24433	13.68245
57	0.08245	0.29058	16.56311	0.10898	0.23686	13.50089
58	0.08110	0.29032	16.83862	0.10819	0.23446	13.59884
59	0.08097	0.28584	16.86465	0.10729	0.23242	13.71306
60	0.08032	0.28337	17.00237	0.10761	0.22788	13.67293
61	0.08145	0.27484	16.76504	0.10308	0.23399	14.27326
62	0.07793	0.28261	17.52205	0.10392	0.22835	14.15763
63	0.07770	0.27898	17.57576	0.10545	0.22147	13.95236
64	0.07504	0.28433	18.19733	0.10084	0.22796	14.58976
65	0.07609	0.27610	17.94667	0.10309	0.21957	14.27200
66	0.07713	0.26826	17.70518	0.10714	0.20808	13.73302
67	0.07851	0.25960	17.39349	0.10329	0.21260	14.24436
68	0.08251	0.24340	16.55091	0.10417	0.20770	14.12380
69	0.07721	0.25631	17.68544	0.10247	0.20809	14.35821
70	0.08099	0.24088	16.86133	0.10283	0.20439	14.30728
71	0.08168	0.23548	16.71889	0.10971	0.18888	13.41070
72	0.07975	0.23783	17.12397	0.10666	0.19159	13.79482
73	0.07844	0.23849	17.40967	0.10800	0.18661	13.62279
74	0.08142	0.22666	16.77269	0.10480	0.18971	14.03859
75	0.07734	0.23542	17.65644	0.10729	0.18285	13.71358
76	0.08071	0.22262	16.91895	0.10658	0.18164	13.80429
77	0.07951	0.22305	17.17516	0.10967	0.17422	13.41499
78	0.07772	0.22525	17.56983	0.10318	0.18282	14.25974
79	0.08092	0.21360	16.87464	0.10740	0.17340	13.69888
80	0.08219	0.20767	16.61375	0.10658	0.17256	13.80519
81	0.07570	0.22271	18.03914	0.10385	0.17490	14.16703
82	0.07456	0.22334	18.31375	0.10881	0.16490	13.52187
83	0.07780	0.21148	17.55266	0.10587	0.16744	13.89762
84	0.07943	0.20467	17.19248	0.10997	0.15927	13.37863
85	0.07897	0.20344	17.29261	0.10550	0.16407	13.94636
86	0.07874	0.20165	17.34225	0.10876	0.15730	13.52771
87	0.08251	0.19024	16.55091	0.10380	0.16292	14.17412
88	0.08240	0.18833	16.57279	0.10247	0.16317	14.35864

Table 2: SSLIC performance as a function of number of threads using 3D color (CIE-Lab) image.

Number of Threads	Without Connectivity			With Connectivity		
	Time (sec)	Efficiency	Speedup	Time (sec)	Efficiency	Speedup
1	7609.695	1.000	1.000	8408.861	1.000	1.000
2	3798.146	1.002	2.004	4188.603	1.004	2.008
4	2043.198	0.931	3.724	2322.334	0.905	3.621
8	1094.085	0.869	6.955	1268.391	0.829	6.630
16	640.219	0.743	11.886	777.877	0.676	10.810
24	462.156	0.686	16.466	568.193	0.617	14.799
32	352.315	0.675	21.599	455.163	0.577	18.474
44	263.890	0.655	28.837	364.519	0.524	23.068
66	244.558	0.471	31.116	339.879	0.375	24.741
88	229.544	0.377	33.151	328.298	0.291	25.614

Table 3: SSLIC execution time as a function of number of threads using 2D color (CIE-Lab) image for the classic ITK threading models and then modern ITKv5 for the Platform, Pool and Intel TBB multi-threader backends with the connectivity step disabled.

Number Of Threads						
	Platform-ITKv5	Platform	Pool-ITKv5	Pool	TBB-ITKv5	TBB
1	1.34867	1.35434	1.33995	1.33794	1.33399	1.33770
2	0.68490	0.69555	0.69927	0.69472	0.69832	0.69568
4	0.38042	0.36096	0.37429	0.35614	0.37650	0.38728
8	0.21055	0.20014	0.20832	0.19859	0.20917	0.20680
16	0.12448	0.12499	0.12277	0.12098	0.12407	0.12199
24	0.08972	0.09700	0.08750	0.08921	0.08905	0.09168
32	0.07299	0.07627	0.07103	0.07583	0.07541	0.09243
44	0.06716	0.08840	0.06633	0.08090	0.06707	0.08494
66	0.06681	0.07791	0.06489	0.07481	0.06552	0.07683
88	0.06612	0.07897	0.06520	0.07814	0.06646	0.07689

Table 4: SSLIC execution time as a function of number of threads using 2D color (CIE-Lab) image for the classic ITK threading models and then modern ITKv5 for the Platform, Pool and Intel TBB multi-threader backends with the connectivity step enabled.

Number Of Threads	Platform-ITKv5	Platform	Pool-ITKv5	Pool	TBB-ITKv5	TBB
1	1.49384	1.48678	1.49108	1.47300	1.48905	1.47446
2	0.78172	0.77497	0.79180	0.76258	0.77926	0.76014
4	0.42666	0.41437	0.42546	0.41542	0.42530	0.42242
8	0.24895	0.23785	0.24425	0.23820	0.24367	0.23841
16	0.15398	0.14963	0.15049	0.15083	0.15281	0.14950
24	0.11750	0.11866	0.11588	0.11687	0.11543	0.11390
32	0.09789	0.10405	0.09599	0.10164	0.09592	0.10590
44	0.09570	0.11320	0.09330	0.11615	0.09358	0.10134
66	0.09016	0.10575	0.08906	0.10324	0.08958	0.10352
88	0.09178	0.10528	0.08576	0.10437	0.08789	0.10294

Table 5: The speed up of the modern ITKv5 implementation of SSLIC compared to the original implementation as a function of number of threads using 2D color (CIE-Lab) image with the connectivity step disabled.

Number Of Threads	Platform/TBB-ITKv5	TBB/TBB-ITKv5	Pool/Pool-ITKv5	Platform/Platform-ITKv5
1	1.01525	1.00278	0.99850	1.00421
2	0.99604	0.99622	0.99350	1.01556
4	0.95873	1.02863	0.95149	0.94886
8	0.95683	0.98869	0.95332	0.95058
16	1.00746	0.98329	0.98545	1.00409
24	1.08933	1.02956	1.01952	1.08117
32	1.01131	1.22566	1.06760	1.04488
44	1.31797	1.26646	1.21963	1.31622
66	1.18914	1.17266	1.15290	1.16616
88	1.18835	1.15696	1.19843	1.19447

Table 6: The speed up of the modern ITKv5 implementation of SSLIC compared to the original implementation as a function of number of threads using 2D color (CIE-Lab) image with the connectivity step enabled.

Number Of Threads				
	Platform/TBB- ITKv5	TBB/TBB- ITKv5	Pool/Pool- ITKv5	Platform/Platform- ITKv5
1	0.99847	0.99020	0.98787	0.99527
2	0.99450	0.97547	0.96311	0.99137
4	0.97430	0.99322	0.97639	0.97120
8	0.97612	0.97841	0.97524	0.95542
16	0.97921	0.97837	1.00227	0.97178
24	1.02801	0.98679	1.00853	1.00989
32	1.08472	1.10396	1.05886	1.06297
44	1.20971	1.08289	1.24491	1.18298
66	1.18049	1.15558	1.15928	1.17297
88	1.19775	1.17124	1.21704	1.14699